

ORIGINAL ARTICLE

Average gap distance between adjacent conductive fillers in polyimide matrix calculated using impedance extrapolated to zero frequency in terms of a thermal fluctuation-induced tunneling effect

Panpan Zhang¹, Yuezhen Bin^{1,2}, Rong Zhang³ and Masaru Matsuo¹

Temperature dependence of conductivity of polymer composites was analyzed using the DC component (frequency \rightarrow 0 Hz) of AC conductivity in terms of thermal fluctuation-induced tunneling through thin barriers to evaluate the average gap distance (D) between adjacent vapor-grown carbon fibers (VGCFs) in a polyimide (PI) matrix. This approach was confirmed to be reasonable in comparison with direct calculation of the D value via the DC measurement. The direct DC measurement provides the average conductivity of the system, whereas the DC component (frequency \rightarrow 0 Hz) of AC conductivity provides two or three types of phase lag mechanisms, the interface between the composites and electrode, the contact region between adjacent VGCFs and the impedance of VGCFs themselves. The best fit between experimental and theoretical frequency dependence of impedance was realized by the equivalent circuit models, which were classified into several phase lags. The D values calculated by the phase lag due to electron charge on adjacent VGCF surfaces were 1.20 and 1.00 nm for the composites with 3.11 and 6.28 VGCF vol% contents, respectively. The D values are independent of temperature from 25 up to 160 °C, which indicates high thermal resistivity of PI.

Polymer Journal (2017) 49, 839–850; doi:10.1038/pj.2017.71; published online 25 October 2017

INTRODUCTION

The conductivity of some materials tends to increase with increasing temperature. This phenomenon has been analyzed using two mechanisms. One is electron hopping^{1–4} and the other is electron tunneling.^{5,6} Electron hopping is thought to be due to two reasons. The first reason is that electron hopping occurs via the sufficient excess of thermal energy associated with excitation of electrons into the conduction band at a high temperature; the second reason is variable range hopping at a low temperature, as proposed by Mott and Davis.¹ In the variable range hopping theory, excited electrons are unable to jump into the conduction band. Instead, they try to find a similar energy state by hopping beyond their nearest neighbors to more distant sites. This is attributed to greater selection of possible electron energy levels. Electron tunneling is a fluctuation-induced tunneling conduction in disordered materials, as proposed by Sheng.⁶ This approach is different from the well-known electron tunneling theory, which is based on the common concept that electrical current is given by the mean barrier height above the Fermi level of the negatively biased electrode, approximated by the generation of the electron charge and voltage across the film at absolute temperature⁵ and the concept that the common tunneling theory is independent of temperature. The

temperature-dependent conductivity is a new approach that was theorized using a fluctuation probability function by Sheng⁶ when the thermal fluctuation field was stronger than the applied field.

By comparing the experimental and theoretical results for the ultrahigh-molecular-weight polyethylene-carbon filler composite,^{7–9} the analysis using electron tunneling was concluded to be more reasonable than electron hopping. Accordingly, the temperature dependence of conductivity (or resistivity) of polymer-conductive filler composites was analyzed using electron tunneling in terms of positive temperature-dependent materials.⁹

Tunneling current, which was effected by DC measurement, was investigated in polyimide (PI) and vapor-grown carbon fiber (VGCF) composites.¹⁰ VGCFs are similar to rigid CFs, which have been used as reinforcing fillers.^{11–17} Namely, the analysis of tunneling effect using VGCFs is more suitable than flexible multiwall carbon nanotubes (MWCNTs).^{8,18,19} PI was used as the matrix as PI is a rigid amorphous polymer with a very low thermal expansion. Very low thermal expansion is important to verify that an increase in conductivity with an increasing temperature is attributed to active electron transfer between adjacent VGCF surfaces, as the gap distance

¹Department of Polymer Science and Materials, Dalian University of Technology, Dalian, China; ²State Key Laboratory of Fine Chemicals, Dalian University of Technology, Dalian, China and ³Hubei Provincial Key Laboratory of Green Materials for Light Industry, Hubei University of Technology, Wuhan, China
Correspondence: Professor M Matsuo, Department of Polymer Science and Materials, Dalian University of Technology, No. 2 Linggong Road, Ganjingzi District, Dalian, Liaoning 116024, China.

E-mail: mm-matsuo@live.jp

Received 10 June 2017; revised 29 August 2017; accepted 11 September 2017; published online 25 October 2017

(D) between adjacent VGCFs may be postulated to be constant and independent of external heating temperature.

Certainly, the D values of polymer-filler composites were obtained from conductivity measured via direct DC measurement. However, AC impedance of polymer-filler composites shows a complicated frequency dependence near the plateau region for the real part and near the dispersion peak for the imaginary part. To provide the best fit between experimental and theoretical results for the composites with 3.11 and 6.28 vol% contents, in this study, the analyses were evaluated using equivalent circuit model with two or three units. The two units are associated with (1) contact region of the interface between the electrode and the composite and (2) contact region between adjacent VGCFs in the composite with a 3.11 VGCF vol% content. The third unit is related to impedance of VGCFs themselves in addition to the above-mentioned two units for the composite with a 6.28 VGCF vol% content. Therefore, conductivity is divided into the contribution from two or three units, in which each unit consists of parallel arrangement of resistivity and capacitance, and a contact phase element (CPE) is introduced.^{20–23}

The conductivity by DC measurement means that the average value of the composite and the detailed analysis is impossible. However, the conductivity at frequency $\rightarrow 0$ Hz by AC measurement provides significant information about the two or three above-mentioned contact regions. Theoretical results by the equivalent circuit model are in good agreement with the experimental results in the given frequency region.

This paper proposes an approach to justify the application of fluctuation-induced tunneling conduction in disordered materials to polymer-filler composites using the AC measurement. To prove this, frequency dependence of impedance (Z^*) is measured for PI/VGCF composites with 3.11 and 6.28 vol% contents at 25, 40, 80, 120 and

160 °C. The parameter fitting to obtain good agreement between theoretical and experimental results was achieved via computer simulation. Using the parameters for Z^* , the further good fitting was confirmed for the complex electrical modulus (M^*) and AC conductivity (κ) and the Cole-Cole plots for Z^* and M^* in the given frequency range.^{24,25} The D values calculated using the conductivity at frequency $\rightarrow 0$ Hz were 1.20 and 1.00 nm for the composites with 3.11 and 6.28 vol% VGCF contents, respectively. These values were consistent with those calculated using the direct DC measurement.¹¹

The above-mentioned process using the equivalent circuit model indicated that the conductivity of sample at frequency $\rightarrow 0$ Hz is attributed to the contact region between adjacent VGCFs in the composite rather than the in the contact region of the metal–semiconductor interface between the electrode and the composite. The contribution of the former was much higher than that of the latter. This indicates that the conductivity measured via direct DC measurement can be directly applied to the evaluation of D value using fluctuation-induced tunneling conduction in disordered materials proposed by Sheng.⁶ This paper is focused on the complicated approach process leading to the above-mentioned conclusion, and the present fundamental investigation will shed light on a number of applications in industrial fields in the near future.

EXPERIMENTAL PROCEDURES

Sample preparation

To pursue excellent dispersion of VGCFs in PI matrix, PI/VGCF composites were prepared via *in situ* polymerization.^{11,15} The fabrication method has been already described elsewhere.¹¹ The monomers pyromellitic dianhydride and 4,4-diaminodiphenyl ether were used in this system.

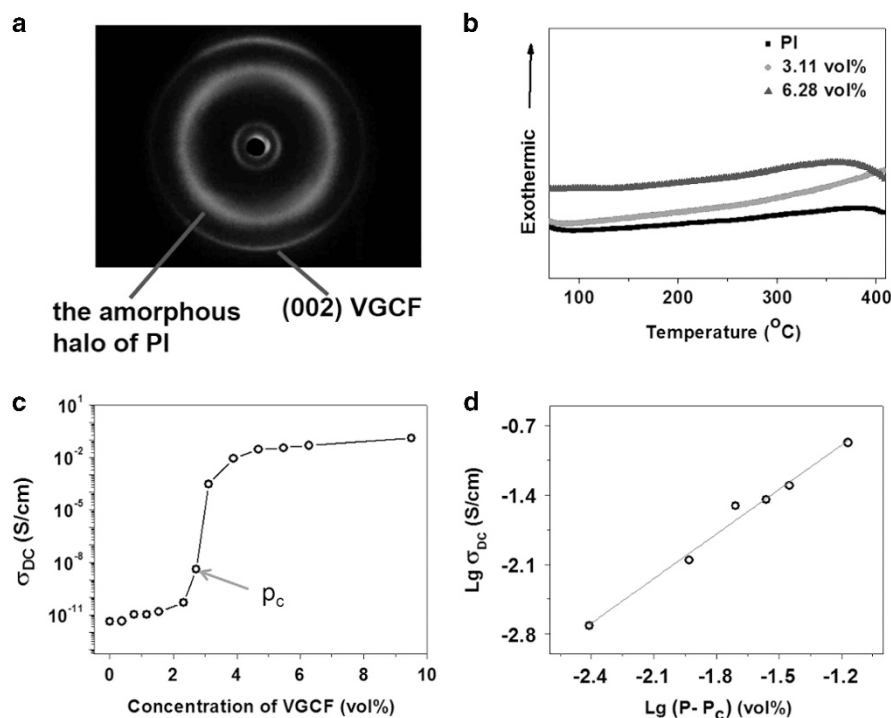


Figure 1 (a) WAXD images of the cross-section of PI/VGCF composite with a 6.28 vol% content. (b) DSC curves of pristine PI and the PI/VGCF composite with 3.11 and 6.28 vol% contents. (c) Logarithmic plots of conductivity versus the VGCF volume content. (d) Plots of conductivity versus $(p - p_c)$ with $p_c = 2.72$ vol%, according to Equation (1). DSC, differential calorimeter; PI, polyimide; VGCF, vapor-grown carbon fiber; WAXD, wide-angle X-ray diffraction. A full colour version of this figure is available at the *Polymer Journal* journal online.

Measurements

The electrical conductivity of the samples was measured using a two-terminal method in which the two ends of the specimen were clamped between copper metal jaws in a hot oven controlled by a commercial program. The temperature was increased from 25 to 170 °C at a rate of 5 °C min⁻¹. Two instruments with different ranges were combined: an R6441A digital multimeter (Advantest, Tokyo, Japan) and an HP 4339B high resistivity meter (Hewlett Packard, Palo Alto, CA, USA) for resistances lower and higher than 107 Ω, respectively. The test piece with a length of 30 mm and a width of 10 mm was cut from the composite film. The sample length clamped between the copper jaws was 10 mm.

The frequency dependence of impedance was measured using a Solartron Impedance/Gain phase Analyzer (Farnborough, Hampshire, UK) (SI1260+1296). The inner plate of Cu electrodes, which was in contact with the composite (specimen), was coated with Au using an

ion coater. Ag paste was coated on the surfaces of the PI/VGCF composite. The measurements were carried out using a circular composite with a diameter of 6.0 mm and a thickness of 0.15~0.17 mm. The bias voltage was set to be 0.1~0.5 V as the scattering degree of impedance at low frequency < 10 Hz was smaller in comparison with that at 0.8 V. The measured frequency was in the range of 10⁻¹ to 10⁶ Hz.

The thermal properties of pristine PI and the composites with 3.11 and 6.28 vol% contents were measured using a differential calorimeter (DSC) from 20 to 410 °C using DSC-Q20 (TA Instruments, New Castle, DE, USA) at a heating rate of 10 °C min⁻¹ in an N₂ atmosphere. Wide-angle X-ray diffraction (WAXD) measurement condition was described elsewhere.¹¹

RESULTS AND DISCUSSION

Figure 1a shows WAXD image for the composite with a 6.28 vol% content ensuring enough contact of adjacent VGCFs. The WAXD

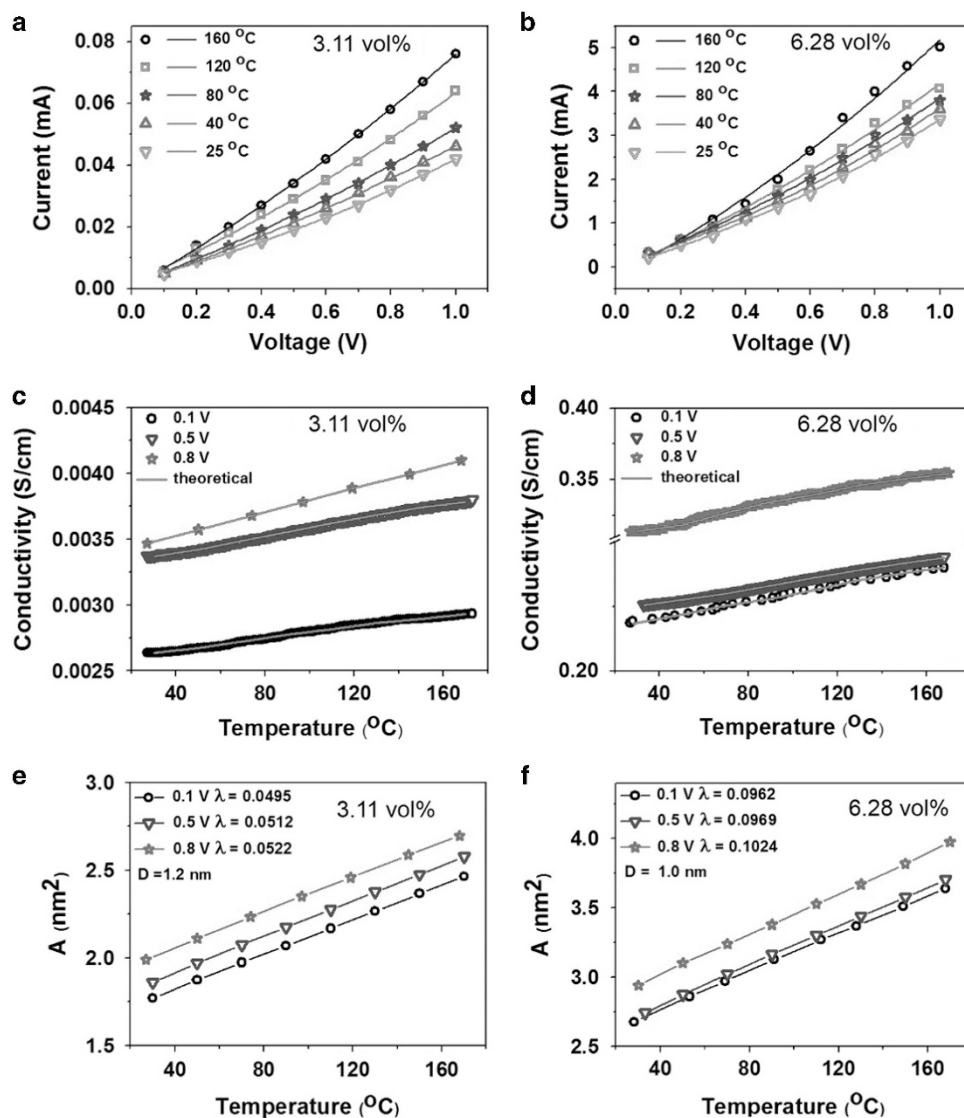


Figure 2 (a, b) Current versus voltage for the PI/VGCF composite with 3.11 vol and 6.28 vol% contents at indicated temperatures. (c, d) Experimental and theoretical conductivities versus temperature for PI/VGCF composites with 3.11 and 6.28 vol% contents at indicated voltages. (e, f) Theoretical value of A versus temperature for composites with 3.11 and 6.28 vol% contents, which were calculated using Equations (2) and (3). PI, polyimide; VGCF, vapor-grown carbon fiber. A full colour version of this figure is available at the *Polymer Journal* journal online.

image showing symmetrical broad arcs in the vertical direction indicates the preferential orientation of VGCFs parallel to the film surface, in which X-ray beam is parallel to the surfaces of the stacked films. Figure 1b shows the DSC results. The curves for the three specimens show a very broad curve with no peak concerning the movement of molecular chains, which indicates that PI molecular chains have good thermal stability below 410 °C. The thermal expansion coefficients of the three specimens from 25 to 200 °C were almost zero, which was already confirmed under a tensile load (~0.06 MPa) when the dynamic tensile modulus was measured.¹¹

Percolation behavior of DC conductivity

Figure 1c shows logarithmic plots of conductivity of the composites versus the VGCF content. The conductivity increased drastically beyond the 2.72 vol% content and leveled off with a further increase in the VGCF content, indicating a percolation phenomenon. In the classical percolation theory,²⁶ the conductivity is related to the volume content as follows:

$$\sigma_{\text{DC}}(p) = \sigma_0(p - p_c)^t \text{ for } p > p_c \quad (1)$$

where $\sigma_{\text{DC}}(p)$ is the composite conductivity, σ_0 is the conductivity of conductive filler, p_c is the percolation threshold, p is the volume content of conductive filler and t is the critical exponent dependent on the dimensions of the lattice and the aspect ratio. In Equation (1), p_c was determined to have a 2.72 vol% content, which is similar to the value (2.2 vol% content) for PI/VGCF composites.²⁷ According to plots of conductivity against $p - p_c$ with $p_c = 2.72$ vol%, as shown in Figure 1d, the value of t obtained from the slope of the regression analysis was determined to be 1.49, which is lower than 1.56 for the PI/MWCNT composites.¹⁵

Following Stauffer and Aharony,²⁸ the exponent t is dependent upon the sample dimensionality, in which $t = 1.1 \sim 1.5$ and $t = 1.6 \sim 1.95$ are reported to be associated with two- and three-dimensional conductive networks, respectively.²⁹ The present value $t = 1.49$ indicates preferential planar orientation of VGCFs in a two-

dimensional space rather than random orientation in a three-dimensional space.

Compared with the analysis using the DC conductivity, the study using dielectric properties as functions of frequency and temperature can supply a lot of information, for example, the formation of conductive filler networks, interface relaxation and polarization.³⁰ Near the percolation threshold ($p \sim p_c$), both the AC conductivity, $\sigma_{\text{AC}}(\omega, p_c)$, and the dielectric constant, $\epsilon(\omega, p_c)$, exhibited frequency dependence. The behaviors are described as $\sigma_{\text{AC}}(\omega, p_c) \sim \omega^x$ and $\epsilon(\omega, p_c) \sim \omega^{-y}$, respectively.³¹ The critical exponents x and y must be satisfied via the relation of $x + y = 1$.

There are two theories related to the frequency dependence of dielectric property.³² Both of them are based on the percolation theory. One is the intercluster polarization effect,^{33–36} which is also called resistor–capacitor model, and the other is the anomalous diffusion inside the clusters.³⁷ In the anomalous diffusion theory, x and y are given as $x = t/\{v(2+\theta)\}$ and $y = (2v - \beta)/\{v(2+\theta)\}$,³⁷ where v , β and θ are the critical exponents that depend primarily on the dimensionality of the percolating system. For a two-dimensional system, the values of v , β and θ are as follows 1.34, 0.14 and 1.00. Substituting them into the above-mentioned equations, we can obtain $x = 0.3885$, $y = 0.6318$ and then $x + y = 1.0203$. For a three-dimensional system, the value of v , β and θ are as follows: 0.9, 0.5 and 1.5. Substituting them into the above-mentioned equations, we can obtain $x = 0.4958$, $y = 0.4127$ and then $x + y = 0.9085$. As we mentioned above, the critical exponents x and y must have the relation of $x + y = 1$. Accordingly, the PI/VGCF composites can be analyzed as a two-dimensional system. Based on the above-mentioned results, the resistor–capacitor model will be discussed later.

Judging from $t = 1.49$ and $x + y = 1$, which are based on two classical percolation theories,^{31–34} the VGCFs are oriented parallel to the film surface. As shown in Figure 1a, the WAXD image indicated the preferential two-dimensional orientation of VGCFs parallel to the film surface. The further detailed discussion for the orientation is described in Supplementary Information. Moreover, the scanning electron microscopy (SEM) images in Supplementary Figures S1a and b reveal that most of the VGCFs are oriented predominantly parallel to the film surface rather than to random orientation in a three-dimensional space, which is in good agreement with $t = 1.49$.

Analysis of DC conductivity using the tunneling effect

Figures 2a and b show current (I) against voltage (V) by external heating in an oven with air-circling. In the given voltage applied at room temperature (25 °C), the self-heating effect by Joule heat was confirmed to be negligible in the preliminary study.¹¹ Then, the indicated temperature is attributed only to external heating. The value of I increased with an increasing temperature at a fixed V . The plots of I versus V curve at the indicated temperatures deviate from the linear relationship, indicating that this relationship is out of the framework of Ohm's law and showing a gradual exponential curve indicating tunneling effect. The fitting parameters at the indicated temperatures are listed in Supplementary Table S1.

Figures 2c and d show temperature dependence of conductivity at the indicated voltages, 0.1, 0.5 and 0.8 V. Voltage was applied at room temperature (25 °C), and conductivity was measured at increasing temperatures, which were produced using external heating at each voltage. Different conductivities were observed at different electrical fields in the given temperature range using external heating. The increase in conductivity with an increasing temperature indicates a tunneling effect, as shown in Figures 2a and b.

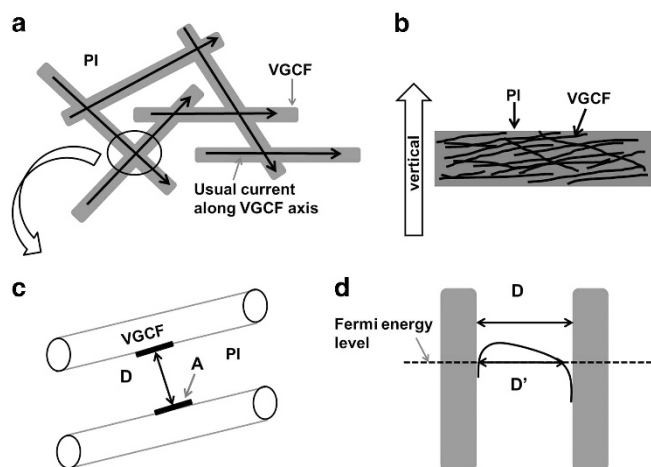


Figure 3 Proposed models to pursue theoretical calculation of resistivity. (a) Model of VGCFs through junction gaps. (b) Model of VGCFs through junction gaps in the composite thickness direction, in which the VGCFs are oriented predominantly parallel to the composite surface. (c) Enlargement of model (a), denoting a gap between neighboring VGCFs with distance D and area A . (d) Potential barrier width (D') at the Fermi energy level is shorter than the distance D between adjacent VGCFs in model (c) under electric field according to Equation (3).¹¹ VGCF, vapor-grown carbon fiber. A full colour version of this figure is available at the *Polymer Journal* online.

Judging from the results in Figures 1 and 2, detailed investigation of the tunneling effect is needed to perform the theoretical calculation. Figure 3a shows the model of VGCFs using junction gaps, and Figure 3b shows the model of VGCFs observed on the cross-section area in the composite. Figure 3c is the enlargement of model (a) for a gap between overlapped VGCFs with an average distance D . A is the average surface area over which most tunneling occurs.^{6,11,38} It is reasonable that most of electron transfers via the tunneling effect are related to D and A . The schematic diagram of the potential barrier shown in Figure 3d is given as a non-parabolic potential function instead of a simple rectangle potential function,^{5,16,39} in which the height of potential barrier becomes lower when D becomes narrower, and A becomes larger with increasing VGCF content.

On the basis of the concept shown in Figure 3, the temperature-dependent conductivity was analyzed using the fluctuation probability function proposed by Sheng⁶ when the thermal fluctuation field is stronger than the applied electrical field. According to Sheng's theory,

E denotes the electron energy in the tunneling direction. The logarithm of the Fermi-Dirac function can be approximated as $-E$ for $E < 0$ and 0 for $E > 0$. As described elsewhere,^{6,11,38} the conductivity σ ($= 1/\rho$, ρ : resistivity) was given as a function of temperature as follows:

$$\sigma = \left(\frac{4T_1}{\pi T}\right)^{1/2} \left\{ \int_0^1 \sum_0(\varepsilon_T) \exp\left[-\frac{T_1}{T}\varepsilon_T^2 - \frac{T_1}{T_0}\varphi(\varepsilon_T)\right] d\varepsilon_T + \int_1^\infty \sum_1(\varepsilon_T) \exp\left(-\frac{T_1}{T}\varepsilon_T^2\right) d\varepsilon_T \right\} \quad (2)$$

where T_1 and T_0 are defined as $DA\delta_0^2/8\pi k$ and $T_1/2\chi D\xi(0)$, respectively, and k is the Boltzmann constant. The parameter $\chi = (8m\pi^2 U_0/h^2)$; where h : Plank's constant) is the tunneling constant, and $\varphi(\varepsilon_T)$ is given by $\xi(\varepsilon_T)/\xi(0)$ and has the properties $\varphi(0) = 1$ and $\varphi(1) = 0$. The complicated derivation of $\xi(\varepsilon_T)$ was described elsewhere^{6,11,17,38} to determine D and A in Figure 3c. ε_T is the dimensionless field parameter given by $\varepsilon_T = \delta_T/\delta_0$, in which δ_T is the thermal fluctuating field, and δ_0 is given by $\bar{\delta}_0 U_0/eD$. U_0 represents the height of the rectangular potential barrier in the absence of an image-force correction, and e is the elementary charge (1.602×10^{-12} erg). $\sum_0(\varepsilon_T)$ at $0 \leq \varepsilon_T \leq 1$ and $\sum_1(\varepsilon_T)$ at $\varepsilon_T > 1$ are formulated as differential tunneling currents by ε_T .⁶ Owing to $\bar{\delta}_0 = (\bar{\delta}/\varepsilon)$, $U(u, \bar{\delta})$ or $U(u, \varepsilon)$, which represent a non-parabolic potential function, is given as follows:

$$U(u, \bar{\delta}) = U_0 \left[1 - \frac{\lambda}{u(1-u)} - \bar{\delta} \right] \\ = U_0 \left[1 - \frac{\lambda}{u(1-u)} - \bar{\delta}_0 \varepsilon u \right] = U(u, \varepsilon) \quad (3)$$

where $u = x/D$ is the reduced spatial variable, in which x is the distance from the left surface of the junction. $\bar{\delta}_0$ is given by $\delta eD/U_0$, in which δ corresponds to δ_T associated with the thermal fluctuation by neglecting the applied field ($\delta_A \rightarrow 0$).⁶ λ is a dimensionless parameter, which is given by $0.795e^2/4DKU_0$ (K : permittivity of the insulating barrier of PI=3.4 (ref. 40)). The potential $U(u, \bar{\delta})$ is a peaked function of u , with a maximum $U_m(u^*, \bar{\delta})$, where u^* satisfies the condition $(\partial U/\partial u) = 0$. Defining $\bar{\delta} = \bar{\delta}_0$ at $U_m = 0$, $\bar{\delta}_0/\lambda$ has a physical meaning at $\lambda \leq 0.25$.^{6,11,17,38} The numerical calculation via computer simulation proved that the partial conductivity of the second term in Equation (2) was negligibly smaller than that of the first term. Then, the numerical calculation discussed below was performed only for $0 \leq \varepsilon \leq 1$.

Returning to Figure 2, the best fitting with the experimental results shown in Figures 2c and d can be realized at $D = 1.20$ nm and $D = 1.00$ nm for composites with 3.11 and 6.28 vol% contents, respectively. The gap distance (potential barrier width) is dependent upon the VGCF content but is independent of the indicated temperatures. This is due to high heat resistance of PI/VGCF composites (see DSC curves in Figure 1b). The dimensionless parameter, $\lambda (= 0.795e^2/4DKU_0)$, is dependent upon voltage but is independent of temperature. Even so, at the same VGCF content, λ increases with increasing voltage, but the degree is not significant. The corresponding results are shown in Figures 2e and f. This indicates that U_0 , which is associated with the height of potential barrier function from Fermi energy level, is almost constant because of the high thermal resistivity of PI/VGCF composites and is independent of the applied field (voltage) in Sheng's theory,⁶ as already discussed.

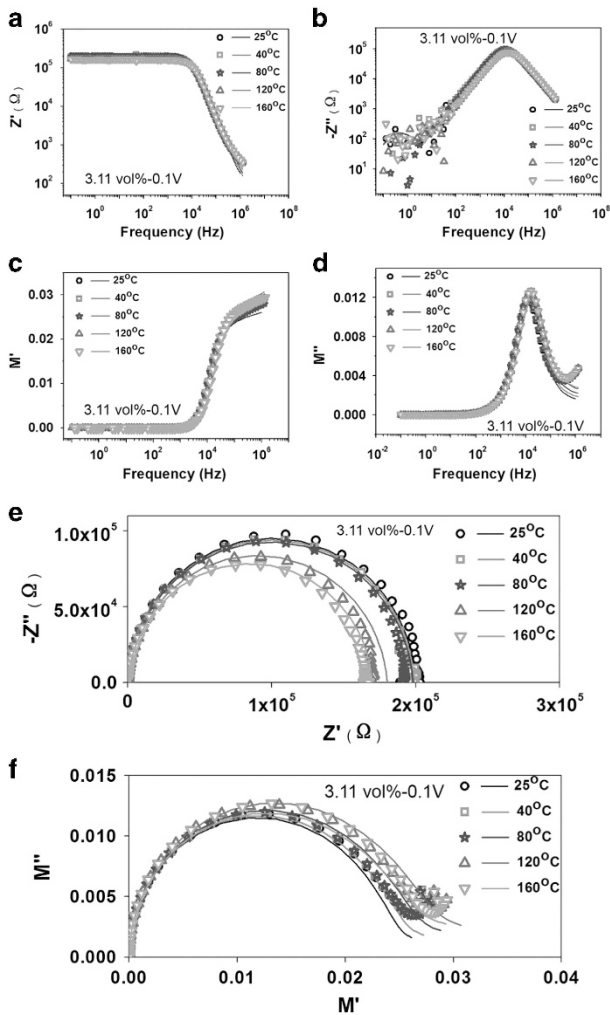


Figure 4 (a, b) Frequency dependence of Z' and Z'' , respectively. (c, d) Frequency dependence of M' ($= C_0\omega Z''$) and M'' ($= C_0\omega Z'$), respectively, where C_0 and ω denote vacuum capacitance and angular frequency, respectively; (e, f) Cole-Cole plots for Z'' and M'' , respectively. Open circles: experimental results. Solid lines: theoretical results. All results at the indicated temperatures were obtained for the composite with a 3.11 vol% content at 0.1 V. A full colour version of this figure is available at the *Polymer Journal* journal online.

Dielectric properties of 3.11 vol% PI/VGCF composites at 0.1 V

To compare the temperature dependence of PI/VGCF composites via DC measurement with the DC component evaluated using the dielectric measurement (AC measurement) in terms of the thermal fluctuation-induced tunneling through thin barriers, frequency dependence of impedance (Z^*) was measured at 0.1 V. Thus, complex permittivity (ϵ^*), complex electric modulus (M^*), AC conductivity (κ) and Cole-Cole plots of M^* and Z^* were calculated using Z^* . These results are shown in Figures 4 and 5.

For Z^* in Figures 4a and b, the results at different temperatures almost overlap. The frequency dependence curves of Z' can be distinguished into two regions: a plateau region below $\sim 10^4$ Hz and a drastically decreasing region beyond $\sim 10^4$ Hz. The frequency of peak appearance for Z'' in Figure 4b is related to the frequency corresponding to the drastic decrease of Z' . The peak of Z'' shifts to higher frequency with an increasing temperature, but the difference is negligibly small. The duller decrease of Z'' at low frequency may consist of several relaxations, although the data are scattered. Actually,

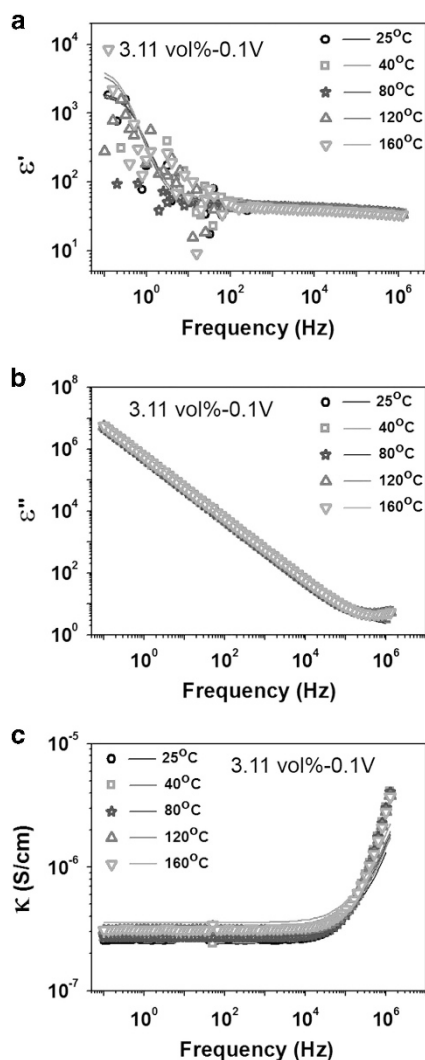


Figure 5 (a–c) Frequency dependence of $\epsilon' (= -Z'' / \{C_0 \omega (Z'^2 + Z''^2)\})$, $\epsilon'' (= Z' / \{C_0 \omega (Z'^2 + Z''^2)\})$ and $\kappa (= \omega \epsilon_0 \epsilon'')$, ϵ_0 : vacuum permittivity), respectively. Open circles: experimental results. Solid curves: theoretical results. All results at the indicated temperatures were obtained for the composite with a 3.11 vol% content at 0.1 V. A full colour version of this figure is available at the *Polymer Journal* journal online.

each Cole-Cole plot of Z^* in Figure 4e shows a circular arc, which is independent of the indicated temperatures but slightly deviates from the arc at the low-frequency side (higher value side of Z').

Regarding the frequency dependence of M' ($= C_0 \omega Z'$) and M'' ($= C_0 \omega Z''$) in Figures 4c and d, respectively, the values of M' show no frequency dependence up to 10^3 Hz. Beyond $\sim 10^3$ Hz, the values increased drastically up to $\sim 10^5$ Hz, and the increasing degree becomes slightly milder beyond $\sim 10^5$ Hz. The corresponding M'' increased drastically beyond $\sim 10^3$ Hz and had a maximum at $1.2 \sim 1.6 \times 10^4$ Hz. The asymmetric shapes of the M'' plots at the indicated temperatures indicate that the dielectric relaxation process deviates from the pure Debye's behavior, and an asymmetric distribution of relaxation time exists. The peak shifted to the higher-frequency side with increasing temperature. However, the shifts were negligibly small. This indicates that the average relaxation time τ_m , which is given by activation energy E_m and pre-exponential factor τ_0 as $\tau_m = \tau_0 \exp(E_m/kT)$, is almost constant. As τ_m is independent of temperature, it is evident that the activation energy of the relaxation processes becomes almost zero.

Furthermore, each peak in Cole-Cole plots for Z^* and M^* appeared at 12 589 Hz in the given temperature range. This tendency is probably because electron transfer via the thermal fluctuation-induced tunneling effect is associated with the same potential barrier width (gap distance) at the indicated temperatures. This is attributed to high heat resistance of PI. In contrast, the E_m and τ_0 for polyvinyl(alcohol)-MWCNT composite with 3 wt% MWCNT²² relating to Maxwell-Wagner-Sillars relaxation⁴¹ were 0.224 eV and $3.162 \times 10^{-19} \text{ s}^{-1}$, respectively. This indicates that there was a strong charge transfer, which was caused by the delocalization of charge carriers accumulated on the interface along a long-range conjugated length.^{42–45} The gap distance between adjacent carbon fillers in a flexible polymer matrix with a large thermal coefficient becomes longer with increasing temperature, and the activation energy then becomes higher despite the predominant electron transfer via the tunneling effect with temperature. The values of E_m for the polyethylene-carbon filler composite with a 23.5 vol% carbon fiber and for 3 wt% poly(vinylalcohol)-MWCNT were reported to be 1.66¹³ and 0.244 eV,²² respectively. In comparison with the E_m values, the value ($E_m \approx 0$) for PI-VGCF indicates the most significant electron transfer with increasing temperature, as the potential barrier width (gap distance) is independent of temperature at least below 200 °C.

Here, we emphasize the significance of M'' in Figure 4d. Generally, in the systems with a conductive component, interfacial relaxation is obscured by conductivity, and dielectric permittivity may be higher at lower frequencies. To overcome this difficulty in evaluating interfacial polarization, the electric modulus formalism is used to study the conductivity relaxation behaviors of the polymer.^{24,25,46} An advantage of adopting the electric modulus to interpret bulk relaxation properties is that variations in the large values of permittivity and conductivity at low frequencies are minimized.

In Figure 5a, the values of the real part of complex permittivity (ϵ') were scattered at the low-frequency region ($< 10^2$ Hz) because of the scattered values of Z'' at the lower-frequency region, and they increased with decreasing frequency, reflecting an interfacial polarization between the composite and the electrode. In contrast, the frequency dependence of the imaginary part of complex permittivity (ϵ'') in Figure 5b appears as clear straight lines below $\sim 10^4$ Hz without scattering because of smooth values of Z' in Figure 4a. The straight lines are attributed to DC conductance. The frequency dependence of ϵ'' beyond $\sim 10^4$ Hz, which denotes the deviation from the straight line, is because of the Maxwell-Wagner-Sillars relaxation or interfacial

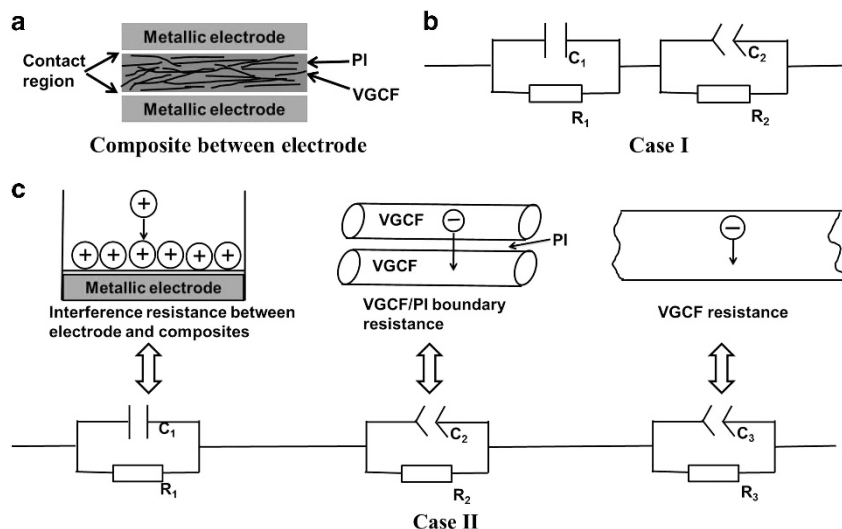


Figure 6 (a) Composite between the electrodes; (b) an equivalent circuit with two units for the 3.11 vol% PI/VGCF composite; (c) an equivalent circuit with three units for the 6.28 vol% PI/VGCF composite. The first unit: interface between the bulk and the electrode; the second unit: interface between adjacent VGCFs inserting PI; the third unit: carrier movement within VGCFs. PI, polyimide; VGCF, vapor-grown carbon fiber. A full colour version of this figure is available at the *Polymer Journal* journal online.

polarization, which refers to the frequency dependence of M'' with a peak at $\sim 2 \times 10^4$ Hz in Figure 4d.

As shown in Figure 5c, the AC conductivity (κ) at the indicated temperatures increases with increasing temperature because of an increase in resistive conduction. Accordingly, it may be expected that the number of transferred electrons between adjacent VGCFs increased via the thermal fluctuation-induced tunneling through thin barriers of PI. The values at the frequency range ($< 10^4$ Hz) corresponding to the DC component are much lower than the results ($0.0026 \sim 0.0035 \text{ S cm}^{-1}$) via direct DC measurement in Figure 2c. This is because of the anisotropy of conductivity, as VGCFs are confirmed to be oriented parallel to the film surface.

To support the concept discussed above, an equivalent circuit model with a serial arrangement of two units is proposed based on the bulk model (shown in Figure 6a) to simulate the dielectric behavior of the composite with a 3.11 vol% content, as shown in Figure 6b.

In Case I, the former represents the contributions from the contact region between the electrode and the composite. The latter represents the adjacent VGCFs in the composite. Each unit consists of two parallel combinations representing two possible electron transfers. One is the current through the resistors, and the other is the current through the capacitors. In addition, the concept of CPE was introduced by Cole^{47–49} to replace the ideal capacitor in the Debye model based on the findings that the measured impedance loci in the complex phase were in the circular arcs with a depressed circle center.

Table 1 Corresponding parameters in Equation (4) and (5) obtained via simulation of the composite with a 3.11 vol% content at 0.1 V at indicated temperatures

T (°C)	25	40	80	120	160
R_1 (Ω)	300	300	300	300	300
C_1 ($F \times 10^{-3}$)	1.10	1.13	1.20	1.99	2.05
R_2 ($\Omega \times 10^4$)	20.0	19.9	19.8	18.0	17.0
C_2 (pF)	89.4	93.4	95.5	97	110
α	0.970	0.965	0.960	0.955	0.950
B	2.031	2.036	2.042	2.047	2.053

CPE is a non-intuitive circuit element. Therefore, impedance is given as follows:

$$Z^* = \frac{1}{\frac{1}{R_1} + i\omega C_1} + \frac{1}{\frac{1}{R_2} + (i\omega)^\alpha C_2} \quad (4)$$

where R_1 and R_2 are resistivities, and C_1 and C_2 are capacitances, in which C_2 is the true capacitance of the contact region associated with CPE. The CPE exponent is given by $\alpha = \phi_{\text{CPE}}/90^\circ$. As the phase angle $\phi_{\text{CPE}} (< 90^\circ)$ is frequency-independent, α is also independent of frequency and is less than 1.0. When α is equal to 1.0, CPE becomes an ideal capacitor. The physical contributions of these parameters in Equation (4) can be proven later via curve fittings with the experimental results. Following Nyikos and Pajkossy,²⁰ α is related to the effective fractal dimension B as follows:

$$\alpha = 1/(B - 1) \quad (5)$$

The theoretical results that provide the best fit for the experimental results are shown as solid curves with different colors in Figures 4 and 5, and the parameters in Equations (4) and (5) are listed in Table 1. As shown in Supplementary Figures S2a and b, the curve separation of the two components providing good fittings revealed that frequency dependence of Z^* is hardly affected by the first term Z_1^* (Z_1' and Z_1'') in Equation S-1 associated with interfacial polarization between the composite and the electrode. Interestingly, the dependence is strongly affected by the second term Z_2^* (Z_2' and Z_2''), which is associated with the polarization between the adjacent VGCFs inserting PI.

As listed in Table 1, the resistance R_1 between the electrode and the composite is constant, which is independent of the temperature. The capacitance C_1 between the electrode and the composite increases with increasing temperature. However, C_1 is much higher than the capacitance C_2 generated by electron charge on the adjacent VGCF surfaces. The slight increase in C_2 with increasing temperature is related to an increase in charged electron numbers between the adjacent VGCF surfaces. Hence, the resistance R_2 slightly decreases via the thermal fluctuation-induced tunneling effect with increasing temperature. The relationship $R_1 \ll R_2$ is attributed to the fact that the contact between Au, which is coated on the electrode plate, and Ag, which is pasted on the composite, is a dense contact region. The

resistance R_1 ($300\ \Omega$) occurred mainly at the contact region between Ag and semi-conductive VGCFs in the composite. The values of B ($2.03 \sim 2.05$) are reasonable because most VGCFs are oriented in the two-dimensional plane.

Figures 4 and 5 provide the discussion for the composite with 3.11 vol% content close to the percolation threshold under 0.1 V. In addition, the experimental and theoretical results under 0.5 V are shown in Supplementary Figures S2c, d and S3 and Supplementary Table S2. The values of parameters in Equation (4) at 0.5 V are slightly different from those at 0.1 V, although the frequency dependence at the indicated temperature provides almost the same tendency.

Dielectric properties for the 6.28 vol% PI/VGCF composites at 0.1 V

Similar to the behaviors of the composite with a 3.11 vol% content in Figure 4a, the frequency dependence of Z' for the composite with a 6.28 vol% content in Figure 7a can be divided into two regions: a plateau region below $\sim 10^4$ Hz and a drastically decreasing region beyond $\sim 10^4$ Hz. The plateau value decreased with increasing temperature, and the decreasing region shifts to the higher-

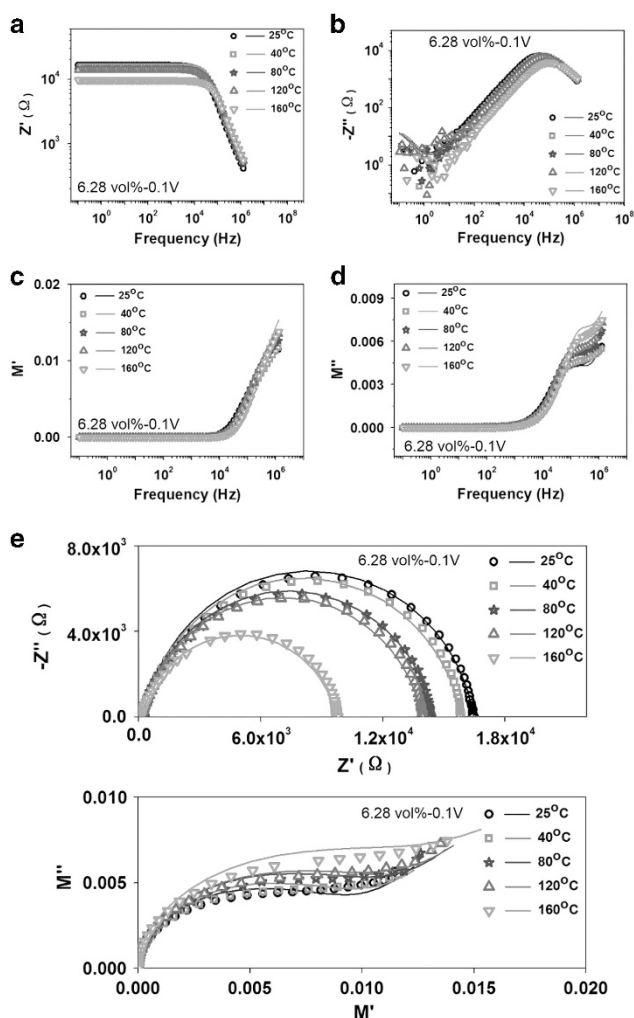


Figure 7 (a, b) Frequency dependence of Z' and Z'' , respectively; (c, d) Frequency dependence of M' and M'' , respectively; (e, f) Cole-Cole plots for Z^* and M^* , respectively. Open circles: experimental results. Solid lines: theoretical results. All results at the indicated temperatures were obtained for the composite with a 6.28 vol% content at 0.1 V. A full colour version of this figure is available at the *Polymer Journal* journal online.

frequency side. The peak frequency for Z'' in Figure 7b is related to the frequency corresponding to a drastic decrease in Z' . The peak shifts to higher frequency, and the peak profile becomes slightly duller with increasing temperature. The values of Z'' tend to level off at low frequency, although the values are scattered. This behavior may indicate the existence of several relaxations. Actually, the Cole-Cole plots of Z^* in Figure 7e show an almost circular arc at the indicated temperatures except for slight deviation in the higher-frequency range (lower value side of Z'). The radius of the circular arc becomes shorter with increasing temperature, which corresponds to the decrease in the magnitude of plateau region of Z' in Figure 7a.

As for M' and M'' , the values of M' show no frequency dependence below 10^3 Hz. Beyond $\sim 10^4$ Hz, the values of M' increased drastically. The corresponding M'' increased drastically beyond $\sim 10^3$ Hz, and the degree of increase becomes milder beyond 10^5 Hz. The asymmetric clear peak of M'' appeared for the composite with a 3.11 vol% content (see Figure 4d), which could not be observed. The Cole-Cole plot of M^* did not form a circular arc, indicating that there were more than two dielectric relaxations.

The profiles of ϵ' , ϵ'' and κ in Figure 8 at the indicated temperatures are essentially similar to those for the composite with a 3.11 vol% content shown in Figure 5. The detailed observation reveals that their magnitude of frequency dependence is more sensitive and higher, and the tendency is considerable at low frequency with increasing temperature. That is, the values of ϵ' increased with decreasing frequency, reflecting interfacial polarization between the composite and the electrode, although they were scattered at low frequency. The frequency dependence of logarithmic plots of ϵ'' appears as a straight line below $\sim 3 \times 10^4$ Hz, denoting a DC component at the indicated temperatures. The κ values in the measured frequency range are much higher than the results of the composite with a 3.11 vol% content. Especially at frequency $< 10^4$ Hz, the plateau values of κ become considerable because of high VGCF content.

To make the complicated relaxation behavior clear, a theoretical calculation was carried out. However, good curve fitting could not be obtained using the equivalent circuit model with two units shown in Figure 6b. Then, Case II with three units is proposed, as shown in Figure 6c. In Case II, the third unit is introduced based on the concept that the resistance of VGCFs may be associated with free movement of charge carriers along the conjugated orbitals in graphene sheets constructing VGCFs. The phase lag of VGCFs themselves cannot be neglected, as the 6.28 vol% content is approximately double in comparison with a 3.11 vol% one. Accordingly, the impedance of the equivalent circuit with three units is given by

$$Z^* = \frac{1}{R_1 + i\omega C_1} + \frac{1}{\frac{1}{R_2} + (i\omega)^\alpha C_2} + \frac{1}{\frac{1}{R_3} + (i\omega)^\beta C_3} \quad (6)$$

The parameter fitting of Z^* in Equation (6) is very important for determining other theoretical phase lags of resistances M^* and ϵ^* . As shown in Figures 7 and 8, the theoretical results for frequency dependences of Z^* , M^* , ϵ^* and κ as well as the Cole-Cole plots of Z^* and M^* are in good agreement with the corresponding experimental results, which confirms the introduction of resistance phase lag of VGCFs themselves. The parameters for giving the best fittings are listed in Table 2.

Each contribution of three terms in Equation (6) to give the best fitting is shown in Supplementary Figures S2e and f. Comparing Figures 7a and b with Supplementary Figures S2e and f, the second term is predominant for providing the best fitting with the experimental results of Z' and Z'' .

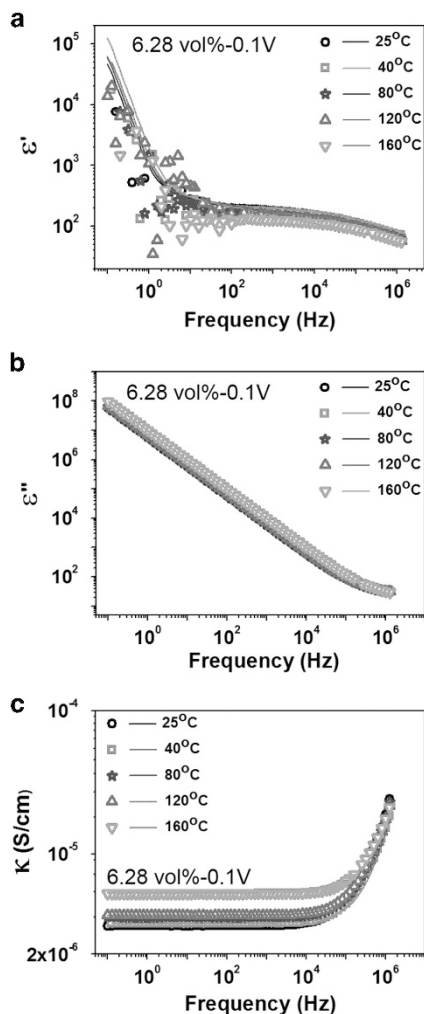


Figure 8 (a–c) Frequency dependence of ϵ' , ϵ'' and κ , respectively. Open circles: experimental results. Solid curves: theoretical results. All results at the indicated temperatures were obtained for the composite with a 6.28 vol % content at 0.1 V. A full colour version of this figure is available at the *Polymer Journal* journal online.

Table 2 Corresponding parameters in Equation (6) obtained from the simulating results for the composite with a 6.28 vol% content at 0.1 V at indicated temperatures

T (°C)	25	40	80	120	160
R_1 (Ω)	30	30	30	30	30
C_1 ($F \times 10^{-3}$)	89.5	89.9	90.0	95.0	100
R_2 ($\Omega \times 10^4$)	1.62	1.55	1.42	1.36	0.94
C_2 (pF)	783	800	793	890	920
α	0.893	0.888	0.883	0.874	0.865
R_3 (Ω)	310	308	306	304	300
C_3 (pF $\times 10^4$)	3.40	3.51	3.80	4.08	4.18
β	0.6548	0.6500	0.6248	0.6304	0.6504

Analysis of the DC component of AC conductivity via the tunneling effect

Returning to Figure 5c for the composite with a 3.11 vol % VGCF content and Figure 8c with a 6.28 vol% content, the theoretical results calculated using Case I with two units in Figure 6b and using Case II with three units in Figure 6c are in good agreement with the

experimental results. Hence, κ_{DC} , corresponding to the DC component (frequency $\rightarrow 0$ Hz) of AC conductivity, is represented as $\epsilon_0/\{C_o(R_1 + R_2)\}$ for the 3.11 vol% VGCF content and $\epsilon_0/\{C_o(R_1 + R_2 + R_3)\}$ for the 6.28 vol % VGCF content. In Case I in Figure 6b, the value of R_2 is much larger than that of R_1 , as listed in Table 1. For Case II shown in Figure 6c, the value of R_2 is much larger than values of R_1 and R_3 , as listed in Table 2. This indicates that conductivity κ_{DC} listed in Table 3 is hardly affected by the first and third units and is governed by the second unit associated with a contact region between adjacent VGCFs. Furthermore, the value of κ_{DC} increases with increasing temperature.

As listed in Table 3, the value of κ_{DC} increases with increasing temperature. Using the κ_{DC} value at the indicated temperatures, the optimum values of D , A and λ are calculated via computer simulation, which is listed in Table 4. Interestingly, the D values calculated using κ_{DC} are the same as the reported values¹¹ obtained using the DC measurement. The D values for the composites with 3.11 and 6.28 vol % contents were 1.20 and 1.00 nm, respectively. The calculated λ values are almost independent of the measured temperatures but they depend on the VGCF contents. At 0.1 V, the λ values for a 3.11 vol% content were 0.0220 independent of temperature, whereas the values (0.02468 ~ 0.02598) for a 6.28 vol% content provide a small dependence on temperature, but the variation can be negligible.

In contrast, as for the DC measurement, the λ values for 3.11 and 6.28 vol% contents were obtained to be 0.0495 and 0.0962 at 0.1 V (shown in Figures 2e and f), respectively. The difference of λ between the two VGCF contents is thought to be the decrease of U_o as the conductivity for the 6.28 vol% content is higher than that for the 3.11 vol% content. However, the values of λ for the DC measurement are higher than those for the AC measurement. This is because for the DC measurement, the electrical field was 0.1 V cm^{-1} (0.1 V per 1 cm, the width between electrodes is 1 cm), whereas for the AC measurement, it was $5.88 \sim 6.67 \text{ V cm}^{-1}$ ($0.1 \text{ V}/(0.015 \sim 0.017 \text{ cm})$), as the width between electrodes is 0.015 ~ 0.017 cm. This is reasonable from the relationship (see Figure 4 in ref. 6 between λ and $\bar{\delta}_o (= VT/D)$) associated with the thermal fluctuation voltage V_T .

At the indicated temperatures, the values of A calculated using κ_{DC} are higher for the 6.28 vol% content than for the 3.11 vol% content. For the two composites, the A values increased with increasing temperature. As the D value is constant, the significant expansion of the average surface area over which most of the tunneling occurs is obviously attributed to an increase in the number of electrons transferred via the thermal fluctuation-induced tunneling effect.^{6,11,32}

Namely, A is related to the number of electrons transferred via the tunneling effect associated with conductivity between adjacent VGCFs inserting PI. The A values calculated by κ_{DC} are much lower than those obtained via the DC measurement, as shown in Figures 2e and f. This is because the DC conductivity along the intrinsic VGCF axis is much higher than that perpendicular to the VGCF axis, as VGCFs are oriented parallel to the composite surface, as previously discussed. This indicates that thermal fluctuation-induced tunneling through thin barriers, which provided reasonable results for DC conductivity, can be applied to the analysis of the DC component of AC conductivity. The equivalent circuit models in Figure 6 confirm that the dielectric measurement at low frequency range gives important information for the morphology of conductive fillers in the polymer matrix.

To obtain additional conclusive evidence, the same treatments at 0.1 V cm^{-1} , shown in Figures 7 and 8, were carried out at 0.5 V , which corresponds to the electric field of $29.4 \sim 33.3 \text{ V cm}^{-1}$ ($0.5 \text{ V}/(0.015 \sim 0.017 \text{ cm})$). In Supplementary Information, the experimental

Table 3 DC components (κ_{DC}) at 0.1 and 0.5 V for the composite with 3.11 vol and 6.28 vol% contents at indicated temperatures

T (°C)	κ_{DC} ($S\ cm^{-1} \times 10^{-7}$; 3.11 vol%) 0.1 V	κ_{DC} ($S\ cm^{-1} \times 10^{-6}$; 6.28 vol%) 0.1 V	κ_{DC} ($S\ cm^{-1} \times 10^{-7}$; 3.11 vol%) 0.5 V	κ_{DC} ($S\ cm^{-1} \times 10^{-6}$; 6.28 vol%) 0.5 V
25	2.557	3.156	3.119	3.663
40	2.703	3.289	3.271	3.853
80	2.717	3.642	3.362	4.161
120	3.066	3.732	3.559	4.686
160	3.098	5.325	3.580	4.954

Table 4 Temperature dependence of parameters D , A and λ at 0.1 and 0.5 V calculated using κ_{DC} shown in Table 3

	T (°C)	λ		D (nm)		A (nm ²)	
		0.1 V		0.5 V		0.5 V	
		0.1 V	0.1 V	0.1 V	0.5 V	0.5 V	0.5 V
3.11 vol%	25	0.02200	1.20	1.621	0.02216	1.20	1.740
	40	0.02200	1.20	1.701	0.02216	1.20	1.752
	80	0.02200	1.20	1.931	0.02216	1.20	1.912
	120	0.02200	1.20	1.941	0.02216	1.20	2.000
	160	0.02200	1.20	1.977	0.02216	1.20	2.135
6.28 vol%	25	0.02468	1.00	2.010	0.02515	1.00	2.360
	40	0.02489	1.00	2.330	0.02531	1.00	2.510
	80	0.02498	1.00	2.430	0.02546	1.00	2.780
	120	0.02501	1.00	2.500	0.02568	1.00	2.860
	160	0.02598	1.00	2.750	0.02582	1.00	2.980

and theoretical results of Z^* are shown in Supplementary Figures S2c and d for the 3.11 vol% content and Supplementary Figures S2g and h for the 6.28 vol% content at 0.5 V. The profiles of frequency dependence for the real and imaginary parts of Z^* at 0.5 V are similar to those at 0.1 V. Accordingly, the profiles for frequency dependence of Z^* , M^* and ϵ^* as well as the Cole-Cole plots of Z^* and M^* at 0.5 V in Supplementary Figures S5 and 6 were similar to the corresponding results at 0.1 V, as shown in Figures 7 and 8. In addition, the values of parameters used in Equation (6) (or Equation S-2) are listed in Supplementary Tables S3. The parameter values at 0.5 V for the 6.28 vol% composite are different from the values at 0.1 V, but the differences are not large.

The values of κ_{DC} at 0.5 V for the composites with 3.11 and 6.28 vol % contents are listed in Table 3 together with the values at 0.1 V. The parameters D , A and λ at 0.1 and 0.5 V, which were calculated using κ_{DC} in Table 3, are listed in Table 4. The D value listed in Table 4 for the composites with 3.11 and 6.28 vol% VGCF contents are 1.20 and 1.00 nm, respectively, at each voltage (0.1, 0.5 V). Judging by the values obtained from the direct DC measurements,¹¹ the D values calculated via the DC component value of AC conductivity are equal to those calculated via conductivity of the direct DC measurement. This indicates that thermal fluctuation-induced tunneling through thin barriers can be adopted to analyze the current mechanism up to 0.5 V. However, in the given frequency range, the Z^* values measured at 0.8 V are scattered, which indicates that an electric field limit exists during the measurement for Z^* .

As listed in Table 4, the values of A for the composites with 3.11 and 6.28 vol% contents become larger with increasing temperature, whereas the value of λ does not significantly change with increasing

temperature. This tendency indicates that the increase in conductivity of the DC component with increasing temperature is attributed to the increase in A denoting average surface area over which most of tunneling occurs.

Using computer simulation for thermal fluctuation-induced tunneling through thin barriers,⁶ two tendencies can be deduced. First, the value of D is very sensitive to $\sigma(T)$ in Equation (2) or $\kappa(T)$ (generally used as κ_{DC} in the present paper) as a function of temperature, and D can thus be uniquely determined. The simulation revealed that when the unsuitable value of D is selected, any good agreement between the experimental and theoretical results cannot be achieved. Second, the values of A and λ are not sensitive compared with D , but they also have an important role in obtaining the best fitting to the experimental values.

Finally, as described elsewhere,^{9,11} we will promote awareness to use the following equation, which has been adopted in many studies.

$$\sigma(T) \propto \exp\left[-\frac{T_1}{T + T_0}\right] \quad (7)$$

Generally, Equation (7) is used in conjunction with a parabolic barrier with the maximum value of the first term $-\left[(T_1/T)\epsilon^2 + (T_1/T_0)\phi(\epsilon)\right]$ in Equation (2) at $\epsilon_T = \epsilon^*$ to estimate the conductivity mechanism for the polymer semi-conductive system as a function of the absolute temperature. Certainly, good fitting between the experimental and theoretical results can also be obtained using Equation (7) similar to Figures 3c and d. However, the calculated D became 0.000200 nm for a 3.11 vol% and 0.000502 nm for a 6.28 vol% content. The values of D at picoscale are clearly out of the physical meaning framework for the distance between adjacent VGCFs. Hence, the theoretical estimation via non-parabolic potential barrier function represented by Equation (3) must be adopted to obtain reasonable analysis.

CONCLUSION

The PI/VGCF composites were fabricated via *in situ* polymerization to realize excellent dispersion of VGCFs in the PI matrix, in which the selected VGCF contents in PI/VGCF composites were 3.11 vol%, which is close to the percolation threshold, and 6.28 vol%, which denotes the maximum content that ensures enough contact with adjacent VGCFs. The predominant orientation of VGCFs parallel to the composite surface was confirmed using the WAXD pattern and scanning electron microscopy imaging. The DC component of AC conductivity was obtained based on the conductivity (frequency \rightarrow 0 Hz) measured at impedance Z^* .

The phase lags of resistances for impedance Z^* were evaluated using an equivalent circuit model with two units for the 3.11 vol% content and using an equivalent circuit model with three units for the 6.28 vol % content, where the CPE was introduced to explain the dielectric behavior of composites in a more reasonable way. The good agreements between experimental and theoretical results were established for the frequency dependence of electric modulus M^* , the

complex permittivity ϵ^* , AC conductivity κ and the Cole-Cole plots of Z^* and M^* , in which the optimum parameters for resistance and capacitance in the above-mentioned circuit models were determined using computer simulation. The DC component κ_{DC} of AC conductivity determined at frequency $\rightarrow 0$ Hz is given by $\epsilon_0/\{C_0(R_1 + R_2)\}$ for the 3.11 vol % content and $\epsilon_0/\{C_0(R_1 + R_2 + R_3)\}$ for the 6.28 vol% content. R_2 , which is associated with the contact region between adjacent VGCFs, is much higher than R_1 , which is associated with the resistance between the electrode and the composite, and R_3 , which is associated with the resistance of VGCFs. This indicates that κ_{DC} is governed by the second unit, which is associated with the contact region between adjacent VGCFs. Actually, the D values calculated using κ_{DC} were 1.20 nm for the 3.11 vol% content and 1.00 nm for the 6.28 vol% content. These values are equal to those evaluated using direct DC measurements. An increase in conductivity of the DC component with increasing temperature was suggested to be attributed to an increase in A denoting the average surface area over which most of tunneling occurs.

Through the analysis of DC component at frequency $\rightarrow 0$ Hz in the AC measurement, it was determined that the thermal fluctuation-induced tunneling through thin barriers is reasonable for the increase in conductivity of PI/VCCF composites, and the introduced equivalent circuit model systems provide important information for the morphology of conductive fillers in the polymer matrix.

CONFLICT OF INTEREST

The authors declare no conflict of interest.

ACKNOWLEDGEMENTS

We are indebted to Professor P Sheng of Hong Kong University of Science and Technology who developed the tunneling effect in many material fields. He kindly taught us how to derive Eq. 14 from Eq. 10, which appeared in ref. 6. We also acknowledge the financial support from the Natural Science Foundation of China (NSFC) program (No 21074016) and (No 21374014).

- Mott, N. F. & Davis, E. A. Disordered materials. (Book reviews: Electronic processes in non-crystalline materials). *Science* **207**, 1196–1197 (1980).
- Okutan, M., Bakan, H. I., Korkmaz, K. & Yakuphanoglu, F. Variable range hopping conduction and microstructure properties of semiconducting Co-doped TiO₂. *Phys. B Condens. Matter* **355**, 176–181 (2005).
- Maddison, D. S. & Tansley, T. L. Variable range hopping in polypyrrole films of a range of conductivities and preparation methods. *J. Appl. Phys.* **72**, 4677–4682 (1992).
- Singh, R. K., Kumar, A., Agarwal, K., Kumar, M., Singh, H. K., Srivastava, P. & Singh, R. DC electrical conduction and morphological behavior of counter anion-governed genesis of electrochemically synthesized polypyrrole films. *J. Polym. Sci. B Polym. Phys.* **50**, 347–360 (2012).
- Simmons, J. G. Electric tunnel effect between dissimilar electrodes separated by a thin insulating film. *J. Appl. Phys.* **34**, 2581–2590 (1963).
- Sheng, P. Fluctuation-induced tunneling conduction in disordered materials. *Phys. Rev. B* **21**, 2180 (1980).
- Bin, Y., Yamanaka, A., Chen, Q., Xi, Y., Jiang, X. & Matsuo, M. Morphological, electrical and mechanical properties of ultrahigh molecular weight polyethylene and multi-wall carbon nanotube composites prepared in decalin and paraffin. *Polym. J.* **39**, 598–609 (2007).
- Chen, Q., Bin, Y. & Matsuo, M. Characteristics of ethylene-methyl methacrylate copolymer and ultrahigh molecular weight polyethylene composite filled with multiwall carbon nanotubes prepared by gelation/crystallization from solutions. *Macromolecules* **39**, 6528–6536 (2006).
- Zhang, R., Bin, Y., Chen, R. & Matsuo, M. Evaluation by tunneling effect for the temperature-dependent electric conductivity of polymer-carbon fiber composites with visco-elastic properties. *Polym. J.* **45**, 1120–1134 (2013).
- Endo, M., Shikata, M., Momose, T. & Shiraiishi, M. *Vapor Grown Carbon Fibers Obtained by Fluid Ultra Fine Catalytic Particles, 17th Biennial Carbon Conference Proceedings*. (American Carbon Society, Lexington, Ky, USA, 1985).
- Zhang, P., Bin, Y., Zhang, R. & Matsuo, M. Joule heat dependence of dynamic tensile modulus of polyimide-vapor grown carbon fiber nanocomposites under applied electric field evaluated in terms of thermal fluctuation-induced tunneling effect. *Polymer* **55**, 2597–2608 (2014).
- Zhu, D., Xu, C., Nakura, N. & Matsuo, M. Study of carbon films from PAN/VGCF composites by gelation/crystallization from solution. *Carbon* **40**, 363–373 (2002).
- Zhu, D., Koganemaru, A., Xu, C., Shen, Q., Li, S. & Matsuo, M. Oxidative stabilization of PAN/VGCF composite. *J. Appl. Polym. Sci.* **87**, 2063–2073 (2003).
- Bin, Y., Mine, M., Koganemaru, A., Jiang, X. & Matsuo, M. Morphology and mechanical and electrical properties of oriented PVA-VGCF and PVA-MWNT composites. *Polymer* **47**, 1308–1317 (2006).
- Jiang, X., Bin, Y. & Matsuo, M. Electrical and mechanical properties of polyimide-carbon nanotubes composites fabricated by *in situ* polymerization. *Polymer* **46**, 7418–7424 (2005).
- Chen, R., Bin, Y., Zhang, R., Dong, E., Uogizawa, T., Kuboyama, K. & Matsuo, M. Positive temperature coefficient effect of polymer-carbon filler composites under self-heating evaluated quantitatively in terms of potential barrier height and width associated with tunnel current. *Polymer* **53**, 5197–5207 (2012).
- Zhang, R., Bin, Y., Dong, E. & Matsuo, M. Considerable different frequency dependence of dynamic tensile modulus between self-heating (joule heat) and external heating for polymer-nickel-coated carbon fiber composites. *J. Phys. Chem. B* **118**, 7047–7058 (2014).
- Koganemaru, A., Bin, Y., Agari, Y. & Matsuo, M. Composites of polyacrylonitrile and multiwalled carbon nanotubes prepared by gelation/crystallization from solution. *Adv. Funct. Mater.* **14**, 842–850 (2004).
- Bin, Y., Chen, Q., Tashiro, K. & Matsuo, M. Electrical and mechanical properties of iodine-doped highly elongated ultrahigh molecular weight polyethylene films filled with multiwalled carbon nanotubes. *Phys. Rev. B* **77**, 035419 (2008).
- Nyikos, L. & Pajkossy, T. Fractal dimension and fractional power frequency-dependent impedance of blocking electrodes. *Electrochim. Acta* **30**, 1533–1540 (1985).
- Sapoval, B. Fractal electrodes and constant phase angle response: exact examples and counter examples. *Solid State Ionics* **23**, 253–259 (1987).
- Zhang, J., Mine, M., Zhu, D. & Matsuo, M. Electrical and dielectric behaviors and their origins in the three-dimensional polyvinyl alcohol/MWCNT composites with low percolation threshold. *Carbon* **47**, 1311–1320 (2009).
- Kaplan, T., Liu, S. & Gray, L. *Fractal Model for the AC Response of a Rough Interface* (Oak Ridge National Lab, TN, USA, 1985).
- Fan, S., Bin, Y., Zhang, R., Zhang, P., Zhu, D. & Matsuo, M. Dielectric change of copper phthalocyanine and polyurethane foam with high elasticity as a function of pressure discussed in terms of conversion from natural mechanical energy to electric energy. *Macromolecules* **47**, 8281–8294 (2014).
- Lv, Z., Wang, Q., Bin, Y., Huang, L., Zhang, R., Zhang, P. & Matsuo, M. Magnetic behaviors of Mg- and Zn-doped Fe₃O₄ nanoparticles estimated in terms of crystal domain size, dielectric response, and application of Fe₃O₄/carbon nanotube composites to anodes for lithium ion batteries. *J. Phys. Chem. C* **119**, 26128–26142 (2015).
- Freilich, S., Gardner, K., Feger, C., Khojasteh, M. & McGrath, J. *Polyimides: Materials Chemistry, and Characterization* (Elsevier, Amsterdam, 1989).
- Ogasawara, T., Ishida, Y., Ishikawa, T. & Yokota, R. Characterization of multi-walled carbon nanotube/phenylethynyl terminated polyimide composites. *Compos. A* **35**, 67–74 (2004).
- Stauffer, D. & Aharony, A. *Introduction to Percolation Theory*. 2nd edn (Taylor and Francis, Bristol, PA, USA, 1992).
- Gefen, Y., Aharony, A., Mandelbrot, B. B. & Kirkpatrick, S. Solvable fractal family, and its possible relation to the backbone at percolation. *Phys. Rev. Lett.* **47**, 1771 (1981).
- Felderhof, B., Ford, G. & Cohen, E. The clausius-mossotti formula and its nonlocal generalization for a dielectric suspension of spherical inclusions. *J. Stat. Phys.* **33**, 241–260 (1983).
- Bergman, D. J. & Imry, Y. Critical behavior of the complex dielectric constant near the percolation threshold of a heterogeneous material. *Phys. Rev. Lett.* **39**, 1222 (1977).
- Song, Y., Noh, T. W., Lee, S.-I. & Gaines, J. R. Experimental study of the three-dimensional AC conductivity and dielectric constant of a conductor-insulator composite near the percolation threshold. *Phys. Rev. B* **33**, 904 (1986).
- Webman, I., Jortner, J. & Cohen, M. H. Critical exponents for percolation conductivity in resistor networks. *Phys. Rev. B* **16**, 2593 (1977).
- Efros, A. & Shklovskii, B. Critical behaviour of conductivity and dielectric constant near the metal-non-metal transition threshold. *Phys. Status Solid. B* **76**, 475–485 (1976).
- Stroud, D. & Bergman, D. J. Frequency dependence of the polarization catastrophe at a metal-insulator transition and related problems. *Phys. Rev. B* **25**, 2061 (1982).
- Wilkinson, D., Langer, J. & Sen, P. N. Enhancement of the dielectric constant near a percolation threshold. *Phys. Rev. B* **28**, 1081 (1983).
- Gefen, Y., Aharony, A. & Alexander, S. Anomalous diffusion on percolating clusters. *Phys. Rev. Lett.* **50**, 77 (1983).
- Zhang, R., Bin, Y., Yang, W., Fan, S. & Matsuo, M. Appearance of perfect amorphous linear bulk polyethylene under applied electric field and the analysis by radial distribution function and direct tunneling effect. *J. Phys. Chem. B* **118**, 2226–2237 (2014).
- Devoret, M. H. & Schoelkopf, R. J. Superconducting circuits for quantum information: an outlook. *Science* **339**, 1169–1174 (2013).
- Alegaonkar, P., Mandale, A., Sainkar, S. & Bhoraskar, V. Refractive index and dielectric constant of the boron and fluorine diffused polyimide. *Nucl. Instrum. Methods Phys. Res. Sec. B* **194**, 281–288 (2002).
- Ku, C. C. & L, D. *Electrical Properties of Polymers* (Hanser Publishers, Munich, 1987).

- 42 Eley, D. Energy gap and pre-exponential factor in dark conduction by organic semiconductors. *J. Polym. Sci. C* **17**, 73–91 (1967)
- 43 Gerhardt, R. Impedance and dielectric spectroscopy revisited: distinguishing localized relaxation from long-range conductivity. *J. Phys. Chem. Solids* **55**, 1491–1506 (1994).
- 44 Cao, W. & Gerhardt, R. Calculation of various relaxation times and conductivity for a single dielectric relaxation process. *Solid State Ionics* **42**, 213–221 (1990).
- 45 Komine, S. Dielectric relaxation study on $\text{Ce}_{0.9}\text{Gd}_{0.1}\text{O}_{1.95}$ ceramics. *Phys. B* **392**, 348–352 (2007).
- 46 Xi, Y., Bin, Y., Chiang, C. & Matsuo, M. Dielectric effects on positive temperature coefficient composites of polyethylene and short carbon fibers. *Carbon* **45**, 1302–1309 (2007).
- 47 Cole, K. S. Electric impedance of suspensions of spheres. *J. Gen. Physiol.* **12**, 29–36 (1928).
- 48 Grimnes, S. & Martinsen, O. Cole electrical impedance model—a critique and an alternative. *IEEE Trans. Biomed. Eng.* **52**, 132–135 (2005).
- 49 MacDonald, J. R. *Impedance Spectroscopy—Emphasizing Solid Materials and Systems*. 1–346 (Wiley-Interscience, John Wiley and Sons, NY, 1987).

Supplementary Information accompanies the paper on Polymer Journal website (<http://www.nature.com/pj>)